Comparison of the embedding and Dyson-equation methods in the Green's-function calculation of a defect in solids

H. Ishida[1] and M. I. Trioni[2]
[1]*College of Humanities and Sciences, Nihon University, Sakura-josui, Tokyo 156, Japan*
[2]*Istituto Nazionale per la Fisica della Materia–UdR Milano Bicocca, via Cozzi 53, 20125 Milano, Italy*
(Received 14 November 2000; published 28 March 2001)

We discuss the relationship between the Dyson-equation method of Wachutka *et al*. [J. Phys. Condens. Matter **4**, 2831 (1992)] and the embedding method of Inglesfield [J. Phys. C **14**, 3795 (1981)] in the Green's-function calculation of a defect in solids. We will show that if the Green's function is expanded using the same basis set, the Green's-function matrix of the embedding method, G^E, is related to that of the Dyson-equation method, G^D, by a simple Dyson-type equation $G^E = G^D + G^D \delta h G^E$, where the matrix δh is related to the incompleteness of the basis set. With the increasing number of basis functions, the Green's functions calculated with the two methods converge to each other rapidly in the interior of the perturbed volume, while they differ persistently on the boundary surface because the Dyson-equation method fails to incorporate the boundary condition of the Green's function. Reflecting this behavior, δh tends to vanish rather slowly with increasing number of basis functions. To demonstrate this, we perform a numerical calculation using a simplified one-dimensional model.

DOI: 10.1103/PhysRevB.63.155108 PACS number(s): 71.15.−m, 71.55.−i, 73.20.Hb

I. INTRODUCTION

Calculating the properties of localized defects in a solid is one of the fundamental subjects in solid-state theory. By virtue of the rapid development of Car-Parrinello-like methods,[1] it is now possible to study the structural properties of single-impurity atoms and crystal surfaces using a huge supercell. However, the supercell technique is not applicable to a number of problems. Among them are the transport properties of defects such as impurity resistivity, for which a precise description of the Fermi surface of a host crystal is prerequisite.[2,3] The Green's-function method is quite suitable for treating those problems, since it can describe a truly isolated defect in an otherwise perfect crystal. Most of the Green's-function methods developed so far are based on the Dyson equation, where the Green's function of a defect-free crystal is computed in the first step to represent the unperturbed system. In the second step the Dyson equation is solved in a localized defect volume either by employing the Korringa-Kohn-Rostoker (KKR) formalism[4,5] or by expanding the Green's function using energy-independent basis functions.[6–9] On the other hand, the embedding approach of Inglesfield[10] is quite unique in its formulation. In his method one concentrates on a defect volume and the effects of the crystal that surrounds it are taken into consideration via the complex potential energy acting on the boundary surface between the defect volume and the rest of the system. The embedding method has been successfully applied to the electronic structure calculation of isolated adsorbates,[11] interfaces,[12] and semi-infinite crystal surfaces.[13–15]

The purpose of the present paper is to discuss the relationship between the Dyson-equation approach and the embedding method of Inglesfield.[10] In particular, we will compare the Green's function constructed using the embedding method and that obtained with the Dyson-equation approach of Wachutka *et al*.[6] In the latter approach, the Dyson equation is cast in matrix form using a nonorthogonal basis set defined in a finite volume with potential perturbation. Also, the embedding equation of Inglesfield[10] is cast in matrix form in actual numerical calculations. Thus, it is very intriguing to explore how the Green's-function matrices of both methods are related to each other when the same basis set is adopted in both calculations. To our knowledge, the work by Baraff and Schlüter[16] is the only one related to this question: They derived a matrix equation, which is equivalent to the Dyson equation but looks more similar to the embedding equation of Inglesfield. The ''embedding'' operator introduced by them plays a role analogous to the true embedding potential. However, as will be shown later, they are not identical. It may be thus desirable if one could compare the two approaches more directly, not only with regard to theoretical formulation, but also from the view point of numerical accuracy.

We will show that the Green's-function matrix of the embedding method, G^E, is related to that of the Dyson-equation method, G^D, by a simple Dyson-type equation $G^E = G^D + G^D \delta h G^E$, where the matrix δh is a property of the basis set and has nothing to do with the perturbation potential. In real space, the Green's functions calculated with the two methods become nearly identical in the interior of the perturbed volume even with a relatively small number of basis functions. However, on the boundary surface, they remain different even with a large number of basis functions, since the Dyson-equation method fails to take into account the boundary condition of the Green's function. As a consequence, the matrix δh converges to zero rather slowly with increasing number of basis functions. To demonstrate this, we perform a numerical calculation using a simplified one-dimensional model for which the exact Green's function can be calculated analytically.

The present paper is organized as follows. In Sec. II we present the theoretical background necessary for discussing

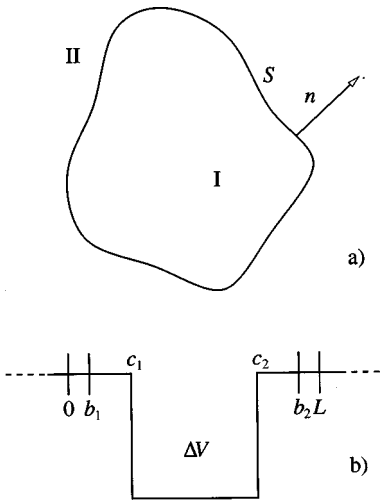

FIG. 1. (a) Schematic picture of a localized defect in a solid. S is the boundary surface between the defect volume I and the rest of the system, II. (b) Box-type defect potential in the one-dimensional free-electron system.

the relationship between the embedding method of Inglesfield and the Dyson-equation approach of Wachutka *et al*. In Sec. III we investigate the convergence of the numerical Green's function to the exact one by performing a numerical calculation. Finally, a summary is given in Sec. IV. Unless stated otherwise, we use Hartree atomic units with $e=m=\hbar=1$ throughout this paper.

II. THEORY

A. Dyson-equation approach

Let us consider a solid described by a one-electron Hamiltonian

$$\hat{H}_0=-\frac{1}{2}\Delta+V_0(\mathbf{r}). \tag{1}$$

We introduce a defect expressed by a perturbation potential $\Delta V(\mathbf{r})$, which is spatially localized in a finite volume I [see Fig. 1(a)]. The electronic structure of the system can be calculated from the Green's function,

$$[\hat{H}-z]g(z,\mathbf{r},\mathbf{r}')=-\delta(\mathbf{r}-\mathbf{r}'), \tag{2}$$

where $\hat{H}=\hat{H}_0+\Delta V(\mathbf{r})$ and z denotes the one-electron energy. In the following we omit the energy suffix z in the Green's function for simplicity. We also consider a Green's function of the unperturbed Hamiltonian $\hat{H}_0$, $g_0(\mathbf{r},\mathbf{r}')$, which is defined in the entire volume I+II and satisfies the outgoing boundary condition at $|\mathbf{r}|=+\infty$ (decaying or propagating toward the infinity). As is well known, $g(\mathbf{r},\mathbf{r}')$ satisfies the Dyson equation

$$g(\mathbf{r},\mathbf{r}')=g_0(\mathbf{r},\mathbf{r}')+\int_{\mathrm{I}}d\mathbf{r}''g_0(\mathbf{r},\mathbf{r}'')\Delta V(\mathbf{r}'')g(\mathbf{r}'',\mathbf{r}'). \tag{3}$$

It is important to stress that the perturbation potential $\Delta V(\mathbf{r})$ is localized in region I, but not the perturbation caused by this potential. The latter is extended in the whole space and $g(\mathbf{r},\mathbf{r}')$ is everywhere different from $g_0(\mathbf{r},\mathbf{r}')$ due to the second term on the right-hand side of Eq. (3). In this spirit, it should be remarked that most of the standard impurity calculations employing the Green's function method concentrate on solving Eq. (3) in the finite region I. But, essentially, one can build its solution in the whole space by, for example, the Green's function matching technique[17] or analytic prolongation.

Assuming that the exact $g_0(\mathbf{r},\mathbf{r}')$ is known, we would like to calculate $g(\mathbf{r},\mathbf{r}')$ by solving Eq. (3). For this purpose, we introduce a basis set $\{\phi_n\}$ defined in volume I and expand the Green function in this volume as

$$g(\mathbf{r},\mathbf{r}')=\sum_{n,n'}(G^D)_{nn'}\phi_n(\mathbf{r})\phi_{n'}^*(\mathbf{r}'). \tag{4}$$

It is to be noted that the expansion (4) is only approximate, as far as we use a finite number of basis functions. For example, in this case, it is impossible to express the cusp in the real part of the Green's function. In order to be able to represent $g(\mathbf{r},\mathbf{r}')$ whose boundary condition on S varies with energy z, $\{\phi_n\}$ should be flexible enough on the boundary surface S between I and II.

Now we follow the formulation of Wachutka *et al.*[6] to cast Eq. (3) in a matrix form. First we try to expand $g_0(\mathbf{r},\mathbf{r}')$ in the same form as Eq. (4),

$$g_0(\mathbf{r},\mathbf{r}')=\sum_{n,n'}(G_0)_{nn'}\phi_n(\mathbf{r})\phi_{n'}^*(\mathbf{r}'). \tag{5}$$

Again, the expansion (5) is only approximate. One possible choice is to obtain $(G_0)_{nn'}$ by minimizing

$$DP_0=\frac{1}{V_{\mathrm{I}}}\left\{\int_{\mathrm{I}}d\mathbf{r}d\mathbf{r}'\left|g_0(\mathbf{r},\mathbf{r}')-\sum_{n,n'}(G_0)_{nn'}\phi_n(\mathbf{r})\phi_{n'}^*(\mathbf{r}')\right|^2\right\}^{1/2}, \tag{6}$$

which is a ''distance'' for the pointwise convergence of the Green's-function expansion to the exact one (V_{I} denotes the volume of region I). From the condition $\partial DP_0/\partial(G_0)_{nn'}^*=0$, one has

$$(G_0)_{nn'}=S_{nm}^{-1}\Gamma_{mm'}S_{m'n'}^{-1}, \tag{7}$$

where S^{-1} denotes the inverse of the overlap matrix $S_{mn}=\int_{\mathrm{I}}d\mathbf{r}\phi_m^*(\mathbf{r})\phi_n(\mathbf{r})$, summation is implied over the repeated indices, and $\Gamma_{mm'}$ is defined by

$$\Gamma_{mm'}=\int_{\mathrm{I}}d\mathbf{r}d\mathbf{r}'\phi_m^*(\mathbf{r})g_0(\mathbf{r},\mathbf{r}')\phi_{m'}(\mathbf{r}'). \tag{8}$$

By substituting Eqs. (4) and (5) into Eq. (3), it is easy to obtain the Dyson equation in a matrix form

$$(G^D)_{nn'}=(G_0)_{nn'}+(G_0)_{nm}\Delta V_{mm'}(G^D)_{m'n'}, \tag{9}$$

$$\Delta V_{nn'} = \int_I d\mathbf{r}\, \phi_n^*(\mathbf{r}) \Delta V(\mathbf{r}) \phi_{n'}(\mathbf{r}). \tag{10}$$

B. Embedding approach

Next, we calculate the Green's function (2) in volume I using the embedding method. According to Inglesfield,[10] the Green's function in volume I satisfies

$$[\hat{H}^E - z] g(\mathbf{r},\mathbf{r}') = -\delta(\mathbf{r}-\mathbf{r}'), \tag{11}$$

where $\hat{H}^E = \hat{H}_0 + \Delta V(\mathbf{r}) + \hat{V}^E$. The last term $\hat{V}^E$, which acts only when $\mathbf{r}$ is located on the boundary surface S, is defined by

$$\hat{V}^E g(\mathbf{r},\mathbf{r}') = \frac{1}{2}\delta(n-n_s) \times \left[\frac{\partial g(\mathbf{x},\mathbf{r}')}{\partial n} - 2\int_S d\mathbf{x}'' \tilde{g}_0^{-1}(\mathbf{x},\mathbf{x}'') g(\mathbf{x}'',\mathbf{r}') \right], \tag{12}$$

where $\mathbf{x}$ is on the boundary surface S and n_s specifies the position of S along the normal coordinate n. In Eq. (12), $\tilde{g}_0^{-1}(\mathbf{x},\mathbf{x}')$ is the surface inverse of $\tilde{g}_0(\mathbf{r},\mathbf{r}')$ over S. Here $\tilde{g}_0$ is a particular Green's function of the unperturbed system $\hat{H}_0$ at energy z, which is defined in volume II (*not* in I), has a vanishing normal derivative on S, and fulfills the outgoing boundary condition at $|\mathbf{r}| = +\infty$. The construction of $\tilde{g}_0$ is more difficult than that of g_0 appearing in Eq. (3) because of the additional boundary condition imposed on S. Here $\tilde{g}_0^{-1}$, which is called *embedding potential*, gives a generalized logarithmic derivative on S of an electron wave function with energy z satisfying the outgoing boundary condition at $|\mathbf{r}| = +\infty$, and $\hat{V}^E$ in $\hat{H}^E$ ensures that the Green's function in I satisfies the correct boundary condition on S.

In volume I we expand the Green's function as

$$g(\mathbf{r},\mathbf{r}') = \sum_{n,n'} (G^E)_{nn'} \phi_n(\mathbf{r}) \phi_{n'}^*(\mathbf{r}'), \tag{13}$$

where $\{\phi_n\}$ is the same basis set as in Eq. (4). Again we notice that the right-hand side of Eq. (13) is only approximate as far as we use a finite number of basis functions. Substituting Eq. (13) into Eq. (11) yields

$$[zS_{lm} - \langle \phi_l | \hat{H}^E | \phi_m \rangle](G^E)_{mn} = \delta_{ln}, \tag{14}$$

which is the original matrix equation derived in the paper of Inglesfield.[10] Given the embedding potential on S, one can calculate also the Green's function of the unperturbed system, $g_0(\mathbf{r},\mathbf{r}')$, by the embedding technique itself. In volume I we expand $g_0(\mathbf{r},\mathbf{r}')$ using the same basis set $\{\phi_n\}$ as

$$g_0(\mathbf{r},\mathbf{r}') = \sum_{n,n'} (G_0^E)_{nn'} \phi_n(\mathbf{r}) \phi_{n'}^*(\mathbf{r}'). \tag{15}$$

Then, G_0^E satisfies

$$[zS_{lm} - \langle \phi_l | \hat{H}_0^E | \phi_m \rangle](G_0^E)_{mn} = \delta_{ln}, \tag{16}$$

where $\hat{H}_0^E = \hat{H}^E - \Delta V$. From Eqs. (14) and (16), it is obvious that the matrices G_E and G_E^0 are related by

$$(G_0^E)_{mn}^{-1} - (G^E)_{mn}^{-1} = \Delta V_{mn} \tag{17}$$

or, equivalently, by the Dyson-type equation

$$(G^E)_{nn'} = (G_0^E)_{nn'} + (G_0^E)_{nm} \Delta V_{mm'} (G^E)_{m'n'}. \tag{18}$$

C. Relationship between G^D and G^E

In order to discuss the relationship between G^E and G^D more clearly, we introduce a matrix

$$\delta h_{mn} \equiv (G_0)_{mn}^{-1} - (G_0^E)_{mn}^{-1}. \tag{19}$$

The matrix δh is related to the incompleteness of the basis set $\{\phi_n\}$ and has nothing to do with the perturbation potential ΔV. If the two expansions (5) and (15) were exact, G_0 and G_0^E must coincide with each other, leading to vanishing δh. In numerical calculations with a small number of basis functions, these expansions are only approximate. Thus, δh does not vanish. However, it may be expected that δh approaches zero gradually as the right-hand side of Eq. (5) and that of Eq. (15) converge to the exact Green's function $g_0(\mathbf{r},\mathbf{r}')$ with increasing number of basis functions.

From Eqs. (17) and (19), we obtain

$$(G^E)_{nn'} = (G_0)_{nn'} + (G_0)_{nm}[\delta h_{mm'} + \Delta V_{mm'}](G^E)_{m'n'}, \tag{20}$$

which coincides with the Dyson equation (9) of Wachutka *et al.*[6] except for the additional term containing δh. Furthermore, from Eqs. (9) and (20), one obtains the equation that directly relates G^D and G^E,

$$(G^E)_{nn'} = (G^D)_{nn'} + (G^D)_{nm} \delta h_{mm'} (G^E)_{m'n'}, \tag{21}$$

and hence

$$(G^D)_{mn}^{-1} - (G^E)_{mn}^{-1} = \delta h_{mn}. \tag{22}$$

Remarkably, Eq. (22) signifies that the difference between the inverse of G^D and that of G^E is independent of the perturbation potential $\Delta V(\mathbf{r})$. Equation (19) may be regarded as a special case of Eq. (22) where $\Delta V(\mathbf{r}) = 0$. As stated above, in actual numerical calculations with a limited number of basis functions, G^D and G^E are not the same because of the nonvanishing term δh in Eq. (21). Hence, an important question that arises is which of the two equations (4) and (13) provides a more accurate description of the Green's function and other related quantities. In the next section, we address this question by performing a numerical calculation using a simplified model system.

Before closing this section, we like to comment on the work of Baraff and Schlüter.[16] Following them, we define an ''embedding'' matrix operator by[18]

$$\Sigma_{mn} = zS_{mn} - \langle \phi_m | \hat{H}_0 | \phi_n \rangle - (G_0)_{mn}^{-1}. \tag{23}$$

Using Eq. (23), the Dyson equation (9) can be written as

$$[zS_{lm}-\langle\phi_l|\hat{H}|\phi_m\rangle-\Sigma_{lm}](G^D)_{mn}=\delta_{ln}. \tag{24}$$

Equation (24) coincides with the embedding equation (14) if Σ is replaced by $\hat{V}^E$. Moreover, Baraff and Schlüter[16] showed that if one adopts a localized linear combination of atomic orbitals (LCAO) basis set, Σ_{mn} is nonvanishing only when both ϕ_m and ϕ_n are located near the boundary surface S. In this sense, Σ is similar to the embedding potential of Inglesfield. However, as seen from Eqs. (19) and (23), Σ and $\hat{V}^E$ are related by

$$(\hat{V}^E)_{mn}=\Sigma_{mn}+\delta h_{mn}, \tag{25}$$

indicating that they become identical only when δh vanishes.

III. NUMERICAL EXAMPLE

To compare the efficiency of the two approaches discussed in the preceding section, we perform an extensive numerical calculation with the use of a simplified one-dimensional model. We consider a one-dimensional free-electron model as the unperturbed system, i.e., $V_0(x)=0$. Thus, the unperturbed Green's function is given simply by a free-electron form $g_0(x,x')=\exp(ik|x-x'|)/(ik)$, where $k=\sqrt{2z}$. As shown in Fig. 1(b), the defect is expressed by a box potential

$$\Delta V(x)=\begin{cases}0 & (x\leqslant c_1, x\geqslant c_2),\\ -v_0 & (c_1\leqslant x\leqslant c_2).\end{cases} \tag{26}$$

We choose a interval $[b_1,b_2]$, which contains $[c_1,c_2]$, as the perturbed volume I. In the terminology of embedding theory, $[b_1,b_2]$ is the embedded region, and the embedding surface corresponds to $x=b_1$ and $x=b_2$. Needless to say, the advantage of employing such a simplified model is that the *exact* Green's function $g(x,x')$ can be analytically calculated, which enables us to evaluate easily the accuracy of the Green's function computed by a numerical method.

As basis function we adopt

$$\phi_n(x)=\sqrt{\frac{2}{L}}\sin(p_n x), \tag{27}$$

where $p_n=\pi n/L$ $(n\geqslant 1)$ and $b_1\leqslant x\leqslant b_2$. In order to be able to represent the Green's function whose boundary condition varies with energy z, the perturbed volume $[b_1,b_2]$ should be taken slightly smaller than $[0,L]$ [see Fig. 1(b)]. As an advantage of the basis set (27), one can systematically improve the accuracy of the basis set by increasing the number of basis functions, N (by increasing the cutoff energy for the plane waves, $E_c=p_N^2/2$). Yet, in contrast to a standard plane-wave band-structure calculation, the maximum N is limited because the basis set is nonorthogonal and becomes overcomplete when N is too large. For the Dyson-equation approach, we first evaluate the matrix element $(G_0)_{mn}$ in Eq. (7) using the exact $g_0(x,x')$, and then, solve Eq. (9) to obtain G^D. The right-hand side of Eq. (4) will be denoted in the following as $g^D(x,x')$. Differently, for the embedding method, we can directly solve Eq. (14) in order to obtain G^E. The Green's function on the right-hand side of Eq. (13) will be denoted as $g^E(x,x')$.

Hereafter we consider energy values slightly above the real energy axis, i.e., $z=\epsilon+i\eta$, where η is an infinitesimal positive number. As a typical example, we will present numerical results for the parameter set: $b_1=1$ a.u., $c_1=3$ a.u., $c_2=7$ a.u., $b_2=9$ a.u., $L=10$ a.u., and $v_0=0.8$ a.u. For these parameters, the numerical calculation is found to be stable up to $N\sim 50$. The basis expansions for $g^D(x,x')$ and $g^E(x,x')$ are meaningful only in the interval $[b_1,b_2]$. Outside this interval, we will plot the analytical extension of each Green's function.[17] For example,

$$g^i(x,x')=\exp[-ik(x-b_1)]g^i(b_1,x'), \tag{28}$$

for $x<b_1$ and $x'>b_1$, and

$$g^i(x,x')=\frac{1}{ik}\exp(ik|x-x'|)+\left[g^i(b_1,b_1)-\frac{1}{ik}\right]\times\exp[-ik(x-b_1)-ik(x'-b_1)], \tag{29}$$

for $x<b_1$ and $x'<b_1$.

In Fig. 2(a) we plot the real part of the Green's function, $\mathrm{Re}\,g(x,x'=5)$ at $\epsilon=0.2$ a.u. as a function of x, where the number of basis functions, N, is only 10, which corresponds to the plane-wave cutoff energy of 9.9 Ry. The exact (analytic) Green's function exhibits a cusp at $x=x'$, whereas the numerical Green's functions $g^D(x,x')$ and $g^E(x,x')$, are not able to describe such a singular behavior. Nevertheless, it is seen that $g^D(x,x')$ and $g^E(x,x')$ reproduce the exact Green's function remarkably well when x is distant from x' even for such a small N. Figure 2(b) shows the local density of states defined by

$$\rho(x,\epsilon)=\frac{-1}{\pi}\mathrm{Im}\,g(\epsilon+i\eta,x,x), \tag{30}$$

where $\epsilon=0.2$ a.u. and $N=10$. Since $\rho(x,\epsilon)$ is a smooth function of x, the agreement between the exact $\rho(x,\epsilon)$ and the corresponding ones computed with the two numerical methods is better than that for the real part of the Green's function in the whole $[b_1,b_2]$ interval. Looking more carefully, one notices that the Green's function—and hence the local density of states—computed with the embedding method mimics the exact values very well also on the boundaries, $x=b_1$ and $x=b_2$, whereas $g^D(x,x')$ and the related $\rho(x,\epsilon)$ deviate from the analytic one to a much larger extent on these boundaries. This behavior is expected, since $\hat{V}^E$ in the embedding Hamiltonian (11) works such that the Green's function may satisfy the correct boundary condition at $x=b_1$ and $x=b_2$. On the other hand, in the Dyson-equation approach, $(G_0)_{mn}$ is determined simply to minimize DP_0 in Eq. (6). Thus, the boundary conditions of the Green's function are not taken into consideration. This different behavior on the boundaries causes a very large deviation of the analytic extension toward region II of the Dyson-equation solution [see Eq. (29)] from the exact one, especially for the local density of states.

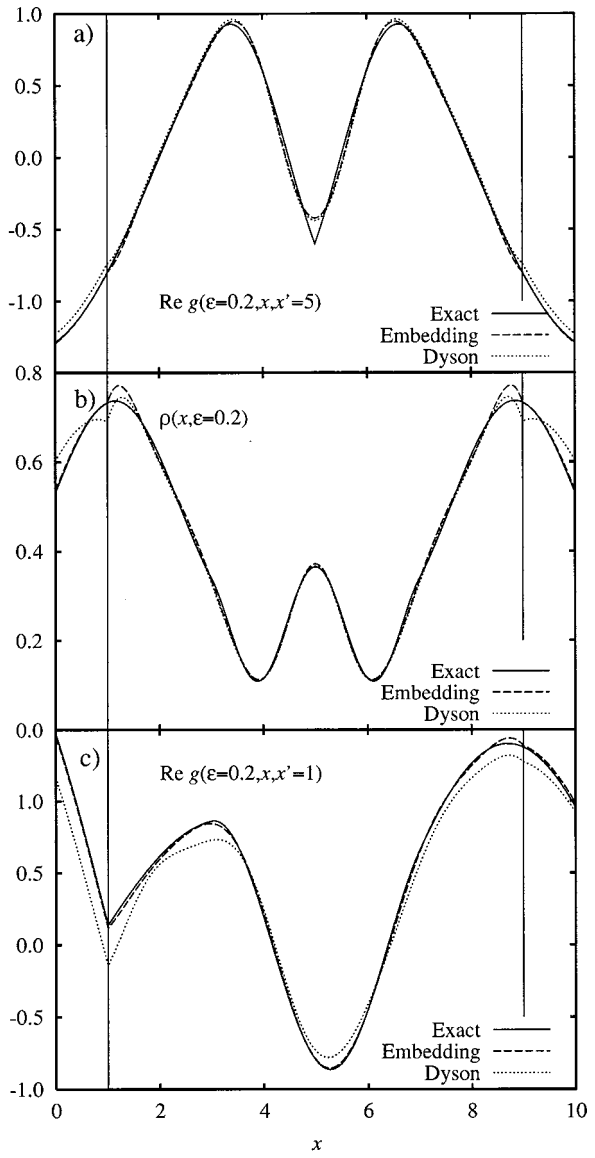

FIG. 2. (a) $\mathrm{Re}\, g(x,x'=5)$. (b) Local density of states $\rho(x,\epsilon)$. (c) $\mathrm{Re}\, g(x,x'=1)$. The solid, dashed, and dotted lines correspond to the analytic Green's function, that computed with the embedding method, and that with the Dyson-equation approach, respectively. $c_1=3$ a.u., $c_2=7$ a.u., $v_0=0.8$ a.u., and $\epsilon=0.2$ a.u., and the number of basis functions, N, is 10.

To examine the behavior of the calculated Green's function near the boundary more clearly, we plot the real part of the Green's function with $x'=b_1$ in Fig. 2(c). Here the boundary conditions in the embedding approach play an essential role to give an extremely better solution with respect to the Dyson-equation approach, also in the interior of the region I.

As seen from Fig. 2, the agreement between the embedding method and the Dyson-equation method is rather good even for a small number of basis functions. As discussed in the preceding section, the two matrices G^E and G^D are related by Eq. (21), indicating that they become identical if δh vanishes. We emphasize again that the matrix δh in this equation is a property of the basis set and has nothing to do

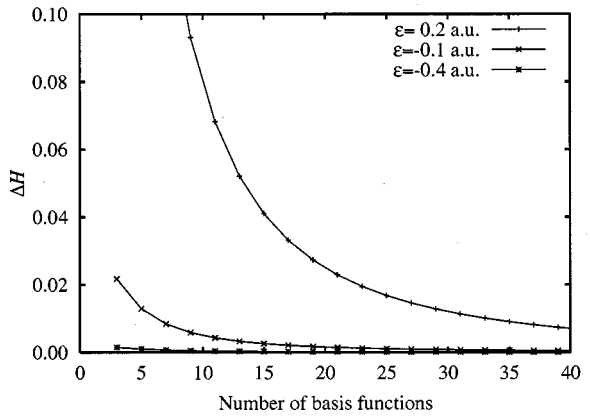

FIG. 3. ΔH as a function of N, the number of basis functions.

with the perturbation potential. Here we examine the behavior of δh as a function of the number of basis functions. Since the absolute value of δh_{mn} has little meaning, we define instead the ratio

$$\Delta H=\sum_{m=1}^{M}\sum_{n=1}^{M}|\delta h_{mn}|\Big/\sum_{m=1}^{M}\sum_{n=1}^{M}|(G_0)^{-1}_{mn}|, \qquad (31)$$

where M is a small integer. In Fig. 3 we plot ΔH ($M=3$) for both positive and negative energies as a function of the number of basis functions, N. As expected, ΔH decreases monotonously with increasing N. However, ΔH converges to zero quite slowly especially for $\epsilon=0.2$ a.u., where ΔH is still $\sim 0.8\%$ at $N=40$.

Now, we discuss how the Green's function calculated using a finite number of basis functions converges to the analytic one with increasing N. For this purpose, we must define a ''distance'' between the exact and numerical Green's functions. Here we consider two different distances: the root mean square distance, which is related to the pointwise convergence, is defined by

$$DP^i=\frac{1}{b_2-b_1}\left\{\int_{b_1}^{b_2}dxdx'|g(x,x')-g^i(x,x')|^2\right\}^{1/2}, \qquad (32)$$

and the ''maximum'' distance, related to the uniform convergence, is defined by

$$DU^i=\sup_{x,x'\in \mathrm{I}}|g(x,x')-g^i(x,x')|, \qquad (33)$$

where index i indicates either D (Dyson) or E (embedding).

Figure 4(a) shows the calculated distances DP^i at $\epsilon=0.2$ a.u. on logarithmic scale as a function of the number of basis functions, N. First, we consider the case of $v_0=0$. In this limiting case, G^E equals G_0^E, and G^D equals G_0 in Eq. (7). Since G_0 is chosen such that DP_0 in Eq. (6) is minimized, the calculated $DP^D(=DP_0)$ is always smaller than DP^E. With increasing N, $g^E(x,x')$ approaches $g^D(x,x')$ rapidly in the interior of the square-shaped integral region in Eq. (32), and as a result, DP^E becomes almost indistinguishable from DP^D on the scale of Fig. 4(a) at around $N\sim 20$ (cutoff energy 39.5 Ry). Next, we consider the case for a finite potential depth v_0. Since the two matrices G^D and G^E satisfy

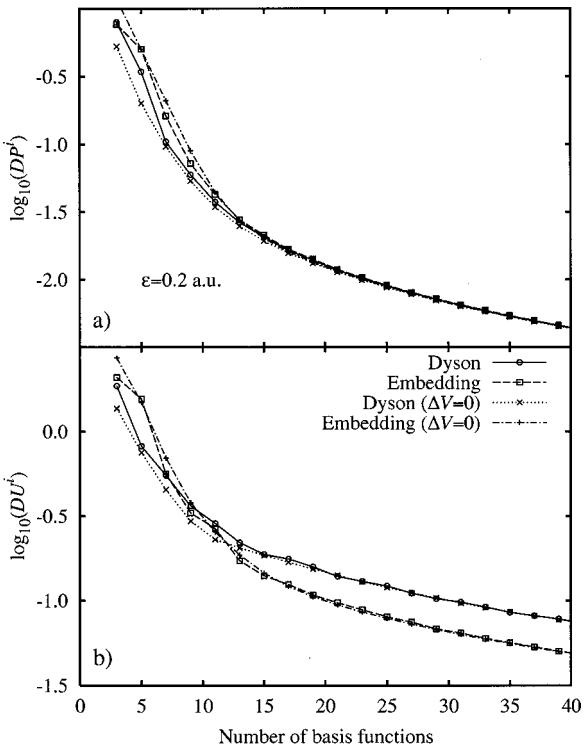

FIG. 4. (a) Root mean square and (b) maximum distance between the analytic and numerical Green's functions as a function of N, the number of basis functions. Energy $\epsilon=0.2$ a.u.

Eqs. (9) and (18), they become the same if G_0 and G_0^E are identical. Hence, at $N\sim 20$ where G_0^E and G_0 become pointwise very close to each other in real space, DP^E becomes almost the same as DP^D for $v_0=0.8$ a.u. For smaller N, $g^E(x,x')$ is slightly less accurate than $g^D(x,x')$ as in the case of $v_0=0$. It is interesting that the four curves in Fig. 4(a) become almost degenerate beyond $N\sim 20$. In this N range, the deviation of the numerical Green's functions from the exact ones becomes independent of the strength of the perturbation potential v_0 and different numerical methods, and is solely governed by the quality of the basis set.

In Fig. 4(b) we show the calculated distances DU^i as a function of the number of basis functions N. Differently from panel (a), the convergence of $g^E(x,x')$ is better than $g^D(x,x')$ over $N\sim 12$, indicating that the former uniformly converges to the exact Green's function faster than the latter. This statement holds true for both cases with and without the perturbation potential v_0. Up to $N\sim 15$, the main contribution to DU^i is due to the cusp of the real part of the Green's function along the line $x=x'$, which cannot be reproduced by numerical calculations with a small number of basis functions. Especially, the convergence of $g^D(x,x')$ with increasing N is terribly slow at the two edge points of this line. Consequently, the main error in $g^D(x,x')$ for larger N arises from the cusps at the two boundary points (b_1,b_1) and (b_2,b_2). As seen from Fig. 2(c), the embedding method can describe the Green's function much better than $g^D(x,x')$ on these boundary points. This explains why the uniform convergence of $g^E(x,x')$ is better than that of $g^D(x,x')$.

In summary $g^E(x,x')$ and $g^D(x,x')$ become nearly identical in the interior of the square region, $b_1\leqslant x,x'\leqslant b_2$, at around $N\sim 20$. However, on the boundary surface, $g^E(x,x')-g^D(x,x')$ exhibits narrow maxima around (b_1,b_1) and (b_2,b_2): Their height decreases with increasing N, but their width also decreases. The coefficients of the Green's functions expansion take into account the global behaviors of such functions. When one expands $g^E(x,x')-g^D(x,x')$ by Fourier series, its high-frequency Fourier components do not vanish. This implies that the two matrices G^E and G^D may approach each other rather slowly with increasing N. In fact, we have observed that $\delta h=(G^D)^{-1}-(G^E)^{-1}$ converges to zero slowly in Fig. 3.

Finally, we would like to comment on the accuracy of the Green's function in numerical calculations for more realistic systems. In the present paper, we have used the exact $g_0(x,x')$ in evaluating the matrix G_0 in Eq. (7). Also, G_0^E in Eq. (16) was calculated using the analytic expression for the embedding potential of the free-electron system. Thus, as stated before, the matrix δh defined by Eq. (19) was related only to the quality of the basis set. For real crystals, one can generally compute neither the exact Green's function $g_0(\mathbf{r},\mathbf{r}')$ nor the exact embedding potential $\tilde{g}_0^{-1}$. Then, the numerical errors in $g_0(\mathbf{r},\mathbf{r}')$ and $\tilde{g}_0^{-1}$ affect the matrices G_0 and G_0^E, respectively, and become an additional source for nonvanishing δh. In this case, it would be difficult to predict which of the Dyson-equation approach and the embedding method provides a more accurate Green's function, since their accuracy depends not only on the basis set $\{\phi_n\}$ but also on the accuracy of the unperturbed Green's function and the embedding potential.

IV. CONCLUSIONS

The embedding formalism of Inglesfiled is unique in the electronic-structure calculation of a defect in solids. So far, its relationship to more popular Green's-function methods based on the Dyson equation was not clarified. In the first half of the present paper, we have discussed the relationship between the two approaches theoretically. Especially, we have shown that if the Green's function is expanded in the localized defect volume using the same basis set, the Green's-function matrix of the embedding method, G^E, and that of the Dyson-equation approach, G^D, satisfy a simple Dyson-type equation $G^E=G^D+G^D\delta h G^E$. The matrix δh in this equation is a property of the basis set and has nothing to do with the perturbation potential. In the second half of the present paper, we conducted an extensive numerical calculation for a simplified one-dimensional model system. We calculated the Green's function of the system using both the embedding method and the Dyson-equation method, and compared them with the exact Green's function.

The main results are the following: We have shown that inside the volume I the Green's functions calculated with the two methods become almost identical with each other at a relatively small number of basis functions. Also, we have found that the embedding method can describe the Green's function more accurately than the Dyson-equation method in

the boundary region of the defect volume. This better description on the boundaries in the embedding approach allows one to find the Green's function in the whole space via, e.g., Green's functions matching, and hence to evaluate many important physical quantities like total energy or dipole moments which require the solution beyond the volume I. To obtain the same accuracy using Dyson-equation approach one must consider a larger volume I in order to match the solutions on a somewhat inner boundary surface, increasing the size of the calculation. On the other hand, as already stated, in the embedding approach the construction of an accurate embedding potential could be a very difficult task.

ACKNOWLEDGMENT

One of the authors (H.I.) would like to thank Professor G. P. Brivio for support during his stay in Milano.

[1] R. Car and M. Parrinello, Phys. Rev. Lett. **55**, 2471 (1985).
[2] R. M. Nieminen and M. Puska, J. Phys. F: Met. Phys. **10**, L123 (1980).
[3] I. Mertig, and E. Mrosan, Phys. Status Solidi B **117**, 619 (1983).
[4] J. Deutz, P. H. Dederichs, and R. Zeller, J. Phys. F: Met. Phys. **11**, 1787 (1981).
[5] V. S. Stepanyuk, W. Hergert, K. Wildberger, R. Zeller, and P. H. Dederichs, Phys. Rev. B **53**, 2121 (1996).
[6] G. Wachutka, A. Fleszar, F. Máca, and M. Scheffler, J. Phys.: Condens. Matter **4**, 2831 (1992).
[7] A. R. Williams, P. J. Feibelman, and N. D. Lang, Phys. Rev. B **26**, 5433 (1982).
[8] P. Krüger and J. Pollmann, Phys. Rev. B **38**, 10 578 (1988).
[9] H. L. Skriver and N. M. Rosengaard, Phys. Rev. B **43**, 9538 (1991).
[10] J. E. Inglesfield, J. Phys. C **14**, 3795 (1981).
[11] M. I. Trioni, S. Marcotulio, G. Santoro, V. Bortolani, G. Palumbo, and G. P. Brivio, Phys. Rev. B **58**, 11 043 (1998).
[12] C. P. Farquhart and J. E. Inglesfield, J. Phys.: Condens. Matter **1**, 599 (1989).
[13] J. E. Inglesfield and G. A. Benesh, Phys. Rev. B **37**, 6682 (1988).
[14] S. Clarke, M. Nekovee, P. K. de Boer, and J. E. Inglesfield, J. Phys.: Condens. Matter **10**, 7777 (1998).
[15] H. Ishida, Surf. Sci. **388**, 71 (1997).
[16] G. A. Baraff and M. Schlüter, J. Phys. C **19**, 4383 (1986).
[17] J. E. Inglesfield, Surf. Sci. **76**, 355 (1978).
[18] To be accurate, Σ_{mn} in (23) is slightly different from the original definition in Ref. 16. In the present work, $(G_0)_{mn}$ is defined by (7). On the other hand, $(G_0)_{mn}$ in Ref. 16 is a subblock of the inverse of a larger matrix, $[zS-\hat{H}_0]_{ij}$, where the indices i and j run not only through basis functions in volume I but also those in volume II.